

Mass Transport Phenomena in a MCFC Cathode

Peter BERG¹ and Justin FINDLAY

Faculty of Science, University of Ontario Institute of Technology,
2000 Simcoe Street N., Oshawa, ON, L1H 7K4, Canada,

¹Email: peter.berg@uoit.ca, Phone: +1 905 721 8668,
FAX: +1 905 721 3304, web: www.peterberg.net

05 August 2009

Abstract

A molten carbonate fuel cell (MCFC) is an electro-chemical energy conversion technology that runs on natural gas and employs a molten salt electrolyte. In order to keep the electrolyte in this state, the cell must be kept at a temperature above 500°C, eliminating the need for precious metals as the catalyst. There has been only a limited amount of research on modelling the transport processes inside this device, mainly due to its restricted applicability for mobile applications.

In this work, three one-dimensional models of a MCFC cathode are presented based on different types of diffusion and convection. Comparisons between models are performed so as to assess their validity. Regarding ion transport, it is shown that there exists a limiting case for ion migration across the cathode that depends on the conductivity for the liquid potential. Finally, an optimization of the diffusivity across the cathode is carried out in an attempt to increase the cell performance and its longevity.

Keywords: molten carbonate fuel cell, mcfc, mathematical modelling, optimization, existence

Nomenclature

b	Bruggeman correction,	1.5	[3, 13, 2]
c	Concentration, mol/m ³		
c_T	Total concentration, mol/m ³		
D	Diffusivity (O ₂ in air), m ² /s	2.5×10^{-5}	
F	Faraday's constant, C/mol	96487	
i_0	Exchange current density, A/m ²	1×10^{-3}	
L	Thickness of cathode, m	8×10^{-4}	[2]
n	Number of electrons in cathode reaction,	4	
P	Pressure		
R	Ideal gas constant, J/K mol	8.314	
T	Temperature, K	900	[1]
u	Fluid velocity, m/s ²		
α	Transfer coefficient,	0.5	[2]
ϵ_g	Gas porosity,	0.4	[2]
ϵ_l	Liquid porosity,	0.3	[2]
ϵ_s	Solid porosity,	0.3	[2]
η	Polarization coefficient, V		
κ	Permeability, m ²	1.9×10^{-12}	[4]
μ	Viscosity, kg/m s	2.25×10^{-5}	[4]
ν	Stoichiometric coefficient		
σ_l	Liquid conductivity, S/m	140	[6]
σ_s	Solid conductivity, S/m	1300	[2]
ϕ	Potential, V		

1 Introduction

Molten Carbonate Fuel Cells (MCFCs) are widely being considered for stationary power generation and a better understanding of the transport processes in the electrodes and cells are needed to improve viability. Recently, a MCFC system was built at Enbridge headquarters in Toronto, Ontario. Their system features four separate MCFC stacks where the primary fuel, natural gas, is pumped into the system from a pressure let-down station. The excess heat released by the fuel cell system is used to heat the adjacent building and preheat the gas before expansion.

Molten carbonate fuel cells were initially developed with the intention of operating directly on coal. The primary fuel currently in use is either coal-derived gases or more commonly natural gas [1]. MCFCs are still under development and have not reached market acceptance as a possible primary or secondary source of energy.

The concept of the MCFC is almost a century old with the first patent awarded in 1916 to W.D. Treadwell. It was first conceived in Europe in the 1940s as an attempt to convert coal to electricity in carbonate media. An initial demonstration was successfully completed by Broers and Ketelaar in the 1950s, with the first pressurized stack appearing in the 1980s. Most of our current knowledge stems from work done in the 1970s and 1980s [1].

Current development concentrates on base-load utility applications as well as dispersed or distributed electric-power generation with heat co-generation. Due to low power densities and long start-up times, there is limited potential for mobile applications, although MCFCs might be suitable for power-trains for large surface ships and trains.

This work presents three mass transport models of a MCFC cathode electrode to be compared for the same parameters. The second section of this work provides a brief introduction to the physical and chemical processes in the cathode electrode. The third section focuses on the three models being used as well as numerical results. Section 4 presents an analytical resolution to the non-existence of numerical solutions found by altering the liquid conductivity parameter based on values in White *et al.* [2]. Section 5 presents an optimization model for the mass transport of a single species in the MCFC cathode electrode. Conclusions will be drawn based on numerical and analytical results in the fifth chapter. Before we begin our analysis, a brief overview of a MCFC cathode is provided and models based on mass transport phenomena shall be described.

2 Cathode

Inside the cathode, oxygen and carbon dioxide flow in the same direction across the electrode at different rates. The three-phase boundary allows for reactions to occur along the length of the domain of the electrode. Across the channel interface, only oxygen and carbon dioxide are able to flow while the liquid electrolyte is kept from flowing into the channel causing corrosion. In fact, the liquid electrolyte distribution is only controlled by capillary pressure. Therefore, the pore size must be maintained very carefully during manufacturing. At the electrode/electrolyte boundary, the electrolyte concentration is much larger and fills the pores, which helps to avoid any gas leakage into the electrolyte assembly.

The inlet gas at the cathode is mainly composed of N_2 , O_2 and CO_2 but contains trace amounts of other molecules since the main source of oxygen comes from air. The effects of nitrogen are neglected in this thesis since it does not flow within the cathode. Only a few metals are stable as a cathode material due to the extremely corrosive nature of the molten carbonate electrolyte and currently nickel oxide is in use. Only semiconducting oxides are feasible from a cost point of view [1]. The mean pore size of NiO electrodes is about $10\ \mu\text{m}$. The smaller pores are filled with

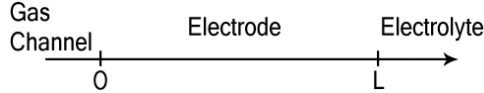


Figure 1: Domain schematic for a one-dimensional cathode electrode.

the electrolyte to form the three-phase boundary needed for the reaction, while the larger pores remain open for gas flow. Nickel oxide is also slightly soluble in the electrolyte which limits the lifetime of the cell, according to



The optimal cathode performance depends upon the gas composition where there exists a 2:1 ratio of CO_2 to O_2 consumed in the overall electro-chemical reaction. In order to reduce the NiO solubility and increase lifetime, the carbon dioxide concentration should be reduced, although if it is too low, the dissociation of carbonate ions becomes significant



thereby limiting the cell lifetime due to electrolyte losses. The balance between NiO solubility and dissociation of CO_3^- can become very difficult to control, and to predict cell lifetime is generally challenging.

The optimal thickness of the electrode, which depends upon the gas composition and current density as well as other operating conditions, ranges from 0.4 – 0.8 mm [1].

At the three-phase boundary in the cathode, oxygen and carbon dioxide diffuse towards the electrolyte which has penetrated the NiO pore. Where the gas flow meets the electrolyte, the gas molecules are absorbed into the electrolyte, react with the electrons at the surface of the electrode, and produce carbonate ions. The electro-chemical reaction is given by



3 Mathematical Models of Diffusion

The diffusion of gases across the cathode of a MCFC are now studied mathematically using three different models. The first model considers only diffusion, while the second and third models consider two different types of diffusion as well as convection.

The electro-chemical reaction in the cathode, Equation (3), involves a reaction between three constituents and the production of another. The reactants diffuse across the cathode from the channel to the electrode/electrolyte boundary (left to right across the domain shown in Figure 1), while the ions also move from left to right. Therefore, a system of four equations will be used that describe the flow of gases, electrons, and ions.

3.1 Fickian Diffusion

The first model is derived using Fick's Laws of Diffusion and Ohm's Law.

The solid and liquid potentials are given by the change in current density using Ohm's Law and the Butler-Volmer equation

$$\frac{d}{dx} \left(\sigma_s \epsilon_s(x)^b \frac{d\phi_s}{dx} \right) = -\nu_s S(\phi_s, \phi_l, c_{O_2}, c_{CO_2}), \quad (4)$$

$$\frac{d}{dx} \left(\sigma_l \epsilon_l(x)^b \frac{d\phi_l}{dx} \right) = \nu_l S(\phi_s, \phi_l, c_{O_2}, c_{CO_2}), \quad (5)$$

where σ_l and σ_s are the conductivities for the liquid and solid phase, respectively. The solid (e^-) conductivity in the MCFC is generally one to two orders of magnitude larger than the liquid (CO_3^{2-}) conductivity, which will create a near constant potential for the former across the domain. The potential is described by ϕ_l and ϕ_s , and determined by the porosity $\epsilon_l(x)$ and $\epsilon_s(x)$, stoichiometric coefficients ν_s and ν_l , and the Butler-Volmer equation, S , describing the reaction kinetics.

Using Fick's Second Law, the rate of change of concentration as a result of diffusion by O_2 and CO_2 and their reaction is found to be

$$\frac{d}{dx} \left(-D \epsilon_g(x)^b \frac{dc_{O_2}}{dx} \right) = -\nu_{O_2} S(\phi_s, \phi_l, c_{O_2}, c_{CO_2}), \quad (6)$$

$$\frac{d}{dx} \left(-D \epsilon_g(x)^b \frac{dc_{CO_2}}{dx} \right) = -\nu_{CO_2} S(\phi_s, \phi_l, c_{O_2}, c_{CO_2}), \quad (7)$$

where D represents the diffusion coefficient, which is the same value for both gas species. Note the exponential dependency on the porosity $\epsilon_g(x)$. The constant b represents the Bruggeman correction for the impedance of diffusion in each phase [3].

The Butler-Volmer equation is given by,

$$S(\phi_s, \phi_l, c_{O_2}, c_{CO_2}) = i_0 c_{O_2} c_{CO_2} e^{\frac{\eta \alpha n F}{RT}}, \quad \eta = \phi_s - \phi_l, \quad (8)$$

where η represents the difference between solid and liquid potentials, n represents the number of electrons in the reaction, and i_0 the exchange current density. The negative exponential term in (8) is dropped since the polarization is at least $\eta > 0.05$ V.

The correction factor for the diffusivities and conductivities are given by the porosity, ϵ_i . The volume fractions must add up to one. If the porosity of two quantities is known, the third quantity is given by,

$$\epsilon_l(x) + \epsilon_g(x) + \epsilon_s(x) = 1. \quad (9)$$

Equations (4)-(7) can be solved numerically using Newton's Method for computational efficiency or iterative methods.

3.2 Fickian Convection-Diffusion

Using a convection-diffusion model, the flux becomes the sum of the convective flux and the diffusive flux. In this model, the molecular interactions are not considered explicitly. They will be included in the third model (Section 3.3).

The convection-diffusion equations for O_2 and CO_2 are given by

$$\frac{d}{dx} \left(u c_{O_2} - D \epsilon_g(x)^b \frac{dc_{O_2}}{dx} \right) = -\nu_{O_2} S(\phi_s, \phi_l, c_{O_2}, c_{CO_2}), \quad (10)$$

$$\frac{d}{dx} \left(u c_{CO_2} - D \epsilon_g(x)^b \frac{dc_{CO_2}}{dx} \right) = -\nu_{CO_2} S(\phi_s, \phi_l, c_{O_2}, c_{CO_2}), \quad (11)$$

where the fluid flux, u , is described by Darcy's Law for porous media,

$$u = -\frac{\kappa\epsilon(x)}{\mu} \frac{dP}{dx} = -\frac{\kappa\epsilon(x)}{\mu} RT \frac{dc_T}{dx}. \quad (12)$$

Compared to the Fickian Diffusion model, there is an extra term and Newton's method is used to solve this type of non-linear problem. Note that the two diffusive fluxes do not necessarily add up to zero.

3.3 Multicomponent Convection-Diffusion

The Maxwell-Stefan equations are used to describe the flux of the diffusing species as well as the interactions between different molecules in the fluid flow. The flux for this model is the sum of the convective flux and the multicomponent diffusive fluxes. The conservation equations for the concentration are given by

$$\frac{d}{dx} \left(uc_{O_2} - D\epsilon_g(x)^b c_T \frac{d}{dx} \frac{c_{O_2}}{c_T} \right) = -\nu_{O_2} S(\phi_s, \phi_l, c_{O_2}, c_{CO_2}), \quad (13)$$

$$\frac{d}{dx} \left(uc_{CO_2} - D\epsilon_g(x)^b c_T \frac{d}{dx} \frac{c_{CO_2}}{c_T} \right) = -\nu_{CO_2} S(\phi_s, \phi_l, c_{O_2}, c_{CO_2}). \quad (14)$$

This model is similar to the model presented in White *et al.* [2], with the addition of convection.

These equations become highly non-linear due to the total concentration term, c_T , which also appears in Darcy's law ($c_T = c_{O_2} + c_{CO_2}$). Newton's Method can be used to solve this model but it is more computationally expensive than the Fickian convection-diffusion model. Note that here the two diffusive fluxes always add up to zero.

3.4 Boundary Conditions

The gas enters the electrode at the channel while the liquid electrolyte penetrates the electrode pores at the opposite side. The gas is unable to flow into the electrolyte due to the pore filling and the electrode is manufactured in such a way as to avoid the corrosive electrolyte penetration of the gas channels.

3.4.1 At the Channel ($x = 0$)

At the channel, the gas is flowing into the electrode. This boundary uses Dirichlet conditions that give the value for the concentration of O_2 and CO_2 as well as the solid potential. The electrolyte is not allowed to move from the electrode into the channel and zero flux is enforced using a Neumann condition for the liquid potential. The boundary conditions are chosen as

$$\phi_s(0) = \phi_{s,0}, \quad \frac{d\phi_l}{dx}(0) = 0, \quad c_{O_2}(0) = c_{O_2,0}, \quad c_{CO_2}(0) = c_{CO_2,0}. \quad (15)$$

In reality, the electrolyte distribution in the cathode is non-uniform and $\epsilon_l(x)$ will be zero for a finite range $0 \leq x \leq x_0$. In fact, $\epsilon_l(x)$ is usually a monotonically increasing function. In essence, we are moving the channel from $x = 0$ to $x = x_0$ in this work since there are no reactions between 0 and x_0 .

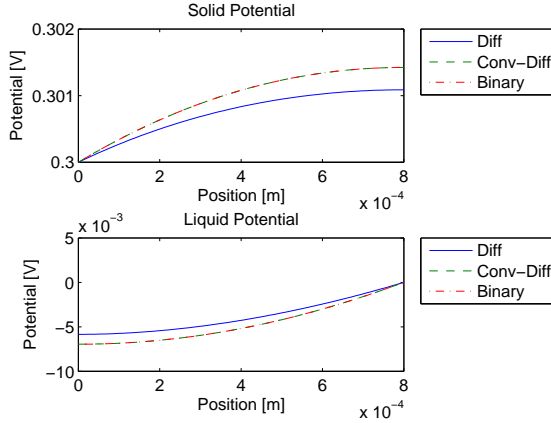


Figure 2: The solid and liquid potential distribution across the electrode using the reference parameters as stated in the nomenclature. The Fickian convection-diffusion (Conv-Diff) and multi-component convection-diffusion (Binary) models share the same profile.

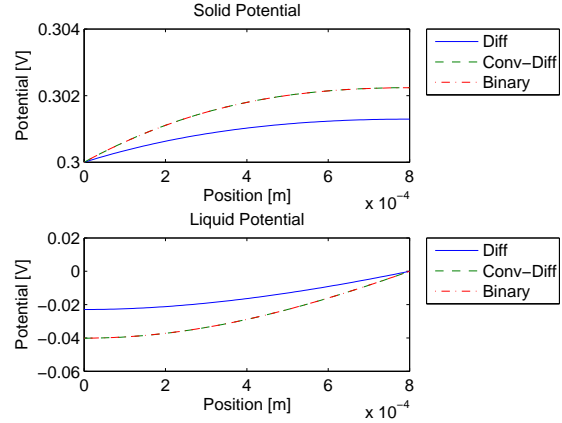


Figure 3: The potential distribution with the liquid conductivity decreased from the reference value of 140 S/m to 50 S/m, which increases the reaction rate.

3.4.2 At the Cathode/Electrolyte Interface ($x = L$)

At the cathode/electrolyte interface, the gas and electrons are not allowed to enter the electrolyte and this is reinforced using Neumann conditions. The liquid potential is given by a Dirichlet condition. These boundary conditions are chosen to be

$$\frac{d\phi_s}{dx}(L) = 0, \quad \phi_l(L) = \phi_{l,L}, \quad \frac{dc_{O_2}}{dx}(L) = 0, \quad \frac{dc_{CO_2}}{dx}(L) = 0. \quad (16)$$

3.5 Results

3.5.1 Solid and Liquid Potential

The potential drop is shown by plotting the solid and liquid phase potentials in Figures 2-5.

The potential difference across the domain using the reference values as in the nomenclature is plotted in Figure 2. The potential remains relatively constant across the domain and all three models remain within one-thousandth of a decimal point in agreement.

The steady state solution for the potential difference, as the liquid conductivity is decreased, is plotted in Figure 3. The liquid conductivity, σ_l , is decreased from 140 S/m to 50 S/m. If the conductivity is decreased further, the steady state solution ultimately does not exist and this will be examined in Section 4. As the liquid conductivity is decreased, the potential gradient increases, hence, the reaction rate increases and since all four equations are coupled, the solid potential and species concentrations also change. This increase is attributed to the inverse relationship between the rate of change in liquid potential and conductivity. The convection-diffusion and multicomponent models share the same profile despite the differences in the formulation. All three models have a change within the same order of magnitude.

The value for the permeability of the MCFC cathode is difficult to obtain but is comparable to that of a Proton Exchange Membrane fuel cell (PEMFC) gas diffusion layer, which contains a

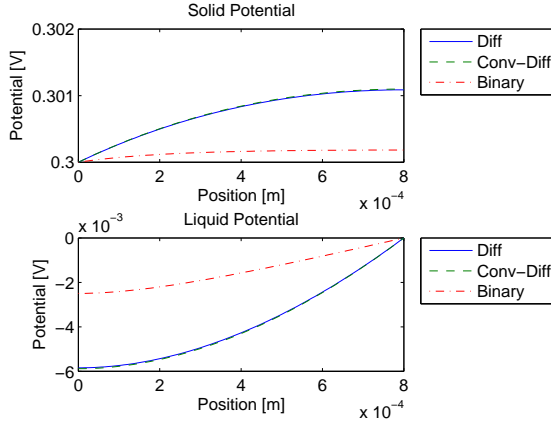


Figure 4: The potential distribution with the permeability decreased three orders of magnitude effectively turning off the convective flux.

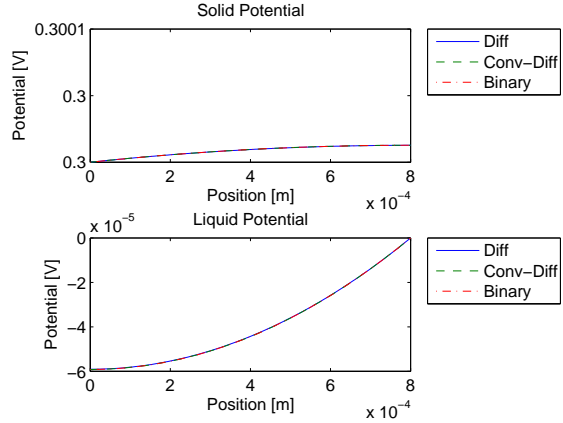


Figure 5: The potential distribution with the exchange current density decreased by two orders of magnitude, slowing the reaction rate. The solid potential varies less than 10^{-3} V across the domain.

similar pore size. The potential difference, when the permeability, κ , is decreased by three orders of magnitude, causing the convective flux to approach zero, is plotted in Figure 4. With the convective flux near zero, the Fickian diffusion and convection-diffusion models are essentially identical and this is shown in the graph as they now share the same profile. The enforcement of zero net diffusive flux in the multicomponent model keeps the potential change lower than that shown by the other models due to the small mass transfer of gas. If the permeability increases, the convective term dominates further and will result in similar results as before.

The exchange current density, i_0 , enters the Butler-Volmer equation and can be found to vary by several orders of magnitude depending on the model. The potential difference is plotted in Figure 5 with the exchange current density at a value of two orders of magnitude less than the reference value, 1.0×10^{-3} A/m², which is the value used in White *et al.* [2]. By decreasing the exchange current density, the reaction rate for each species decreases and the rate of change decreases as well. At such low reaction rates, each model shares the same profile across the domain.

3.5.2 Concentration

The change in concentration of O₂ and CO₂ is plotted in Figures 6-9, corresponding to the results for the potential difference.

The convection term dominates the diffusion term for O₂ across the electrode as it pushes the gas towards the electrolyte as in Figure 6, using the reference values in the nomenclature. This can be seen due to the increase in O₂ concentration as it approaches the cathode/electrolyte boundary. With convection dominating, there is less than a 10% change in concentration, while the Fickian diffusion model without convection shows a 10-20% change in O₂ and CO₂ concentration.

Considering the concentration of O₂, it increases across the domain due to convection and it is not possible to approximate the convection-diffusion profile using an effective diffusivity for the Fickian diffusion model as in White *et al.* [2], which did not include convection.

The steady state solution for a decrease in the liquid conductivity, σ_l , is shown in Figure 7. The value is decreased by an order of magnitude and if decreased further, the steady state solution does not exist (see Section 4) and the code no longer converges. Since the system of four differential equations is coupled, the gradient of the concentration of the gas-species changes along with the

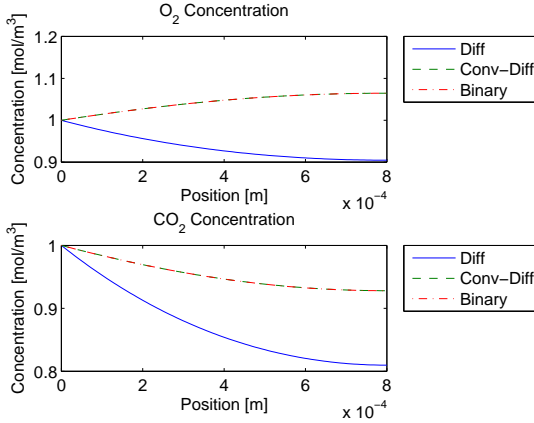


Figure 6: The O_2 and CO_2 concentration profiles across the electrode using the reference values. The Fickian convection-diffusion (Conv-Diff) and multi-component convection-diffusion (Binary) models share the same profile.

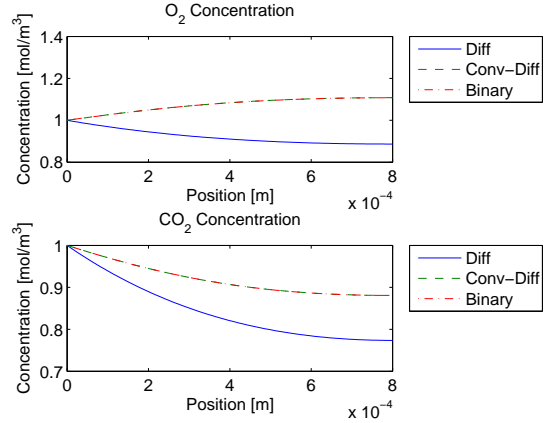


Figure 7: The concentration profiles with the liquid conductivity decreased from the reference value of 140 S/m to 50 S/m, which increases the reaction rate for the liquid potential.

changes in reaction rate. The convective flux remains dominant and the convection-diffusion and multicomponent models continue to share the same profile.

The concentration profile is shown in Figure 8 when the permeability, κ , is decreased by three orders of magnitude. Since the convection is close to zero, diffusion dominates and the Fickian diffusion and convection-diffusion models are essentially the same as was described previously for the potential difference. The differences between the convection-diffusion and multicomponent models becomes more apparent as the concentration drops almost 80% across the cathode using the latter model, while less than 20% for the former model. This can be attributed to maintaining a non-zero convective flux. The discrepancy between the two models will be further analyzed in Section 3.5.4.

The exchange current density, i_0 , when decreased by two orders of magnitude, decreases the reaction rates for all species. As the reaction rate decreases, less species react at the three-phase boundary and the concentration drop is minimal across the domain. With the permeability at the standard value, convection dominates even with low reaction rates. Once again, this is the value of the exchange current density reported in White *et al.* [2]. It still shows the convection term dominating which must be considered in the mass transport of the MCFC cathode.

It should be pointed out here that the model by White *et al.* [2] is ill-posed in that it neglects convection while keeping binary-diffusion terms. Since the latter add up to zero, we cannot have a net flux of gas across the electrode, an obvious contradiction, which they do not discuss. This can be seen by adding (13) and (14) giving (for $u = 0$),

$$\begin{aligned} \frac{d}{dx} \left(-D\epsilon_g(x)^b c_T \frac{d}{dx} \left(\frac{c_{O_2}}{c_T} + \frac{c_{CO_2}}{c_T} \right) \right) &= -(\nu_{O_2} + \nu_{CO_2}) S(\phi_s, \phi_l, c_{O_2}, c_{CO_2}), \\ &= \frac{d}{dx} \left(-D\epsilon_g(x)^b c_T \frac{d}{dx} (1) \right) = 0, \end{aligned} \quad (17)$$

which is a contradiction since S is not identically zero.

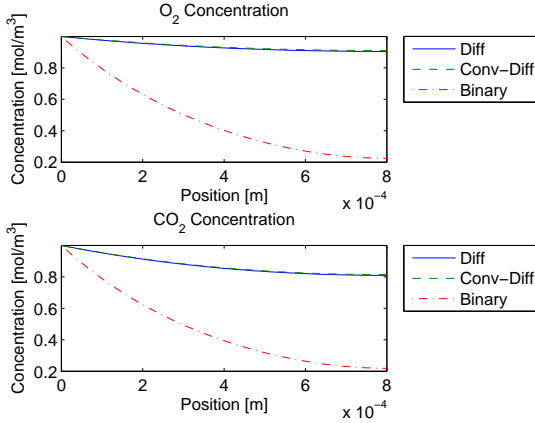


Figure 8: The concentration profiles with the permeability decreased three orders of magnitude, effectively turning off the convective flux.

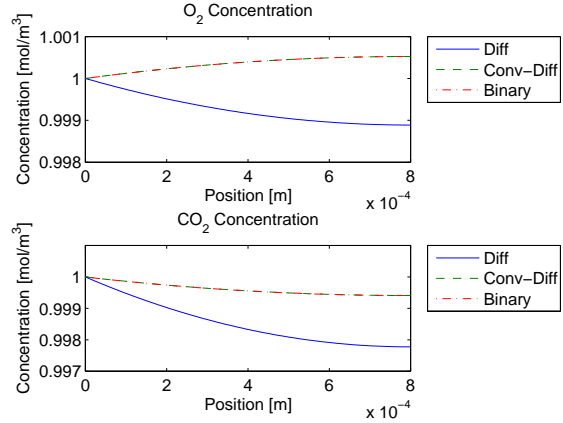


Figure 9: The concentration profiles with the exchange current density decreased by two orders of magnitude, slowing the reaction rate.

3.5.3 Cell Performance

The MCFC operates at current densities in the range of $100 - 200 \text{ mA/cm}^2$ with a cell potential of $0.75 - 0.90 \text{ V}$. Figure 10 shows the polarization curve for the convection-diffusion model at several different values of the diffusivity, D . As the diffusivity decreases, the polarization curve loses its linear character as the degree of irreversibility increases. At the standard reference value for the diffusivity, $2.5 \times 10^{-5} \text{ m}^2/\text{s}$, the cell operates in the appropriate range for the current density and potential difference. This graph was made using an open-circuit or reversible cell potential of $E_r = 1.0 \text{ V}$, which is appropriate for MCFCs [2]. The expected cell polarization for the half-cell reaction in the cathode is shown in the figure as a box.

3.5.4 Comparison of Convection-Diffusion Models

In many cases, researchers in the field of porous media flow are interested in approximating the convection-diffusion equation by using only Fickian diffusion with an effective diffusivity that will provide a similar profile with convection excluded. In the case when the convection term is included along with Fickian diffusion, the concentration of O_2 can increase from the channel to the electrolyte when convection is in the opposite direction of diffusion. Due to this increase, it is not possible to use an effective diffusivity that will provide the same profile since diffusion will only cause the concentration to decrease across the domain. This means that convection must be included in the mass transport of the MCFC cathode and can not be neglected as in White *et al.* [2].

Another area of interest in the study of mass transport in fuel cells is the comparison between the convection-diffusion model of Section 3.2 and the multicomponent convection-diffusion model of Section 3.3. Depending upon the parameters, it is possible that Fick's Law can provide a sufficient description of diffusion across a domain. Note that in the first model, the diffusive fluxes do not add up to zero whereas in the second model they do.

The permeability, κ , is a measure of the ability of a fluid to move through a porous medium. It can be very difficult to measure the permeability of a material for fuel cells as it is directly related to the manufacturing of the material. Values for permeability in the literature for MCFCs have not been found but we can safely use the values for the permeability in the proton exchange membrane fuel cells (PEMFC), which is the primary fuel cell in use for mobile applications. Currently, there

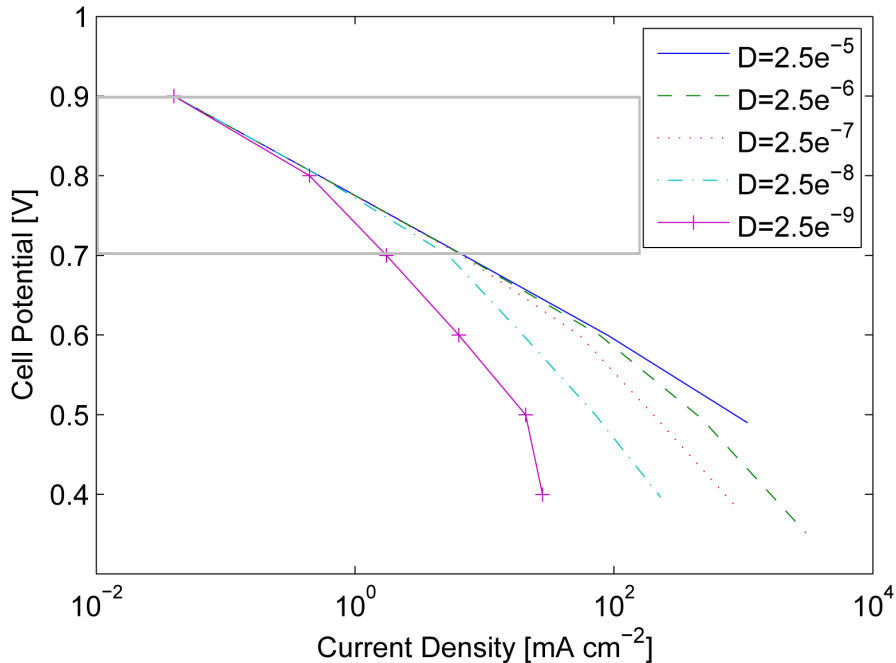


Figure 10: Cell potential versus current density: polarization curve for the half cell Fickian convection-diffusion model.

exists only 2-3 manufacturers of MCFCs and values for the permeability are hard to come by. The pore size in the cathode of the PEMFC is approximately $10 \mu\text{m}$, which is close to that of the MCFC. Realistically, we can determine the permeability of the MCFC to be close to $1.9 \times 10^{-12} \text{ m}^2$ as in the PEMFC model of Promislow *et al.* [4].

The diffusion coefficients in the convection-diffusion model are the same for any number of species considered using Fick's First Law of Diffusion. In the Stefan-Maxwell formulation, only $n-1$ fluxes are independent and for $n > 2$, the diffusion coefficients consist of a matrix. The diffusion coefficients for the species in the cathode of the MCFC are also difficult to find from literature. For instance, White *et al.* [2] state the diffusion coefficients to be $1.16 \times 10^{-4} \text{ m}^2/\text{s}$, which is referenced from Cussler [5, 2], but the diffusion of O_2 through air, which is the highest possible diffusivity, is only $0.25 \times 10^{-4} \text{ m}^2/\text{s}$. The value reported in Fehribach *et al.* [6], $4.3 \times 10^{-6} \text{ m}^2/\text{s}$, is much more realistic.

Due to the uncertainty of values for the permeability and diffusivities, a comparison between the two models for different values is performed so as to validate the use of the convection-diffusion equations as an approximation to the Stefan-Maxwell equations. The convection-diffusion model is far less computationally expensive than the more non-linear multicomponent convection-diffusion model, which will be beneficial for scaling-up the model to higher dimensions.

Figure 11 shows the difference (error) between the O_2 concentration profiles of the Fickian convection-diffusion and multicomponent convection-diffusion models.

The error is calculated as the L^2 -norm of the difference between the O_2 concentration profiles of the Fickian convection-diffusion (fed) and multi-component convection-diffusion (mcd) models

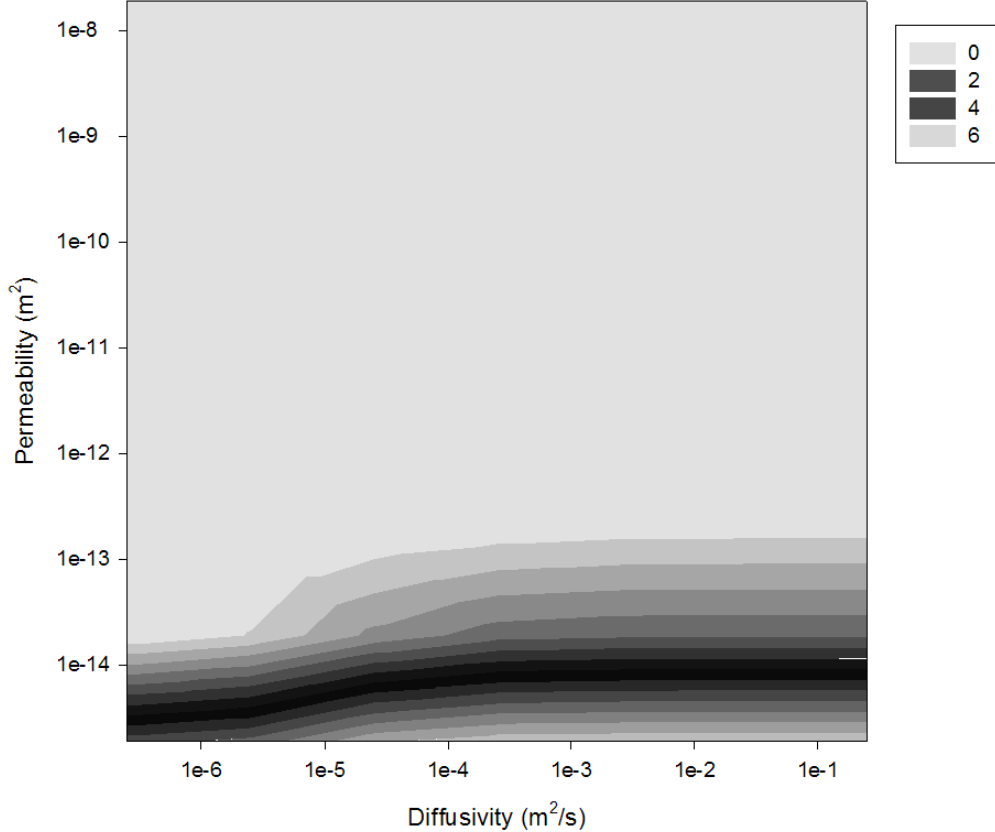


Figure 11: The difference between the concentration profiles for both convection-diffusion and multi-component transport models. For the standard values of both diffusivity, D , and permeability, κ , the error between the solutions is minimal. The error increases for smaller values of the permeability where the convection term is closer to zero. The colours represent the error between profiles and is less than 10^{-5} up to permeabilities less than 1×10^{-13} , where the error grows above 1.

normalized by the area under the O_2 convection-diffusion profile, so that

$$\text{error} = \frac{\left(\int_0^L |c_{O_2}^{fcd} - c_{CO_2}^{mcd}|^2 dx \right)^{1/2}}{\int_0^L c_{O_2}^{fcd} dx}, \quad (18)$$

where Simpson's rule was used to find the area.

For permeability values above $10^{-13} m^2$, there is a very small difference between the profiles (less than 10^{-5}). For smaller values of the permeability, the difference increases significantly. However, for realistic values based on the known diffusivities from the MCFC literature and permeabilities from the PEMFC literature, the convection-diffusion model is in very good agreement with the multicomponent model.

Based on these results, it seems justified to approximate the multicomponent model by using the simpler, and computationally less expensive, convection-diffusion model in MCFC cathode electrodes. This is beneficial for scaling-up the model to higher dimensions as well as in stack models where run time increases dramatically.

4 Fickian Diffusion: Non-Existence of Steady-State Solutions

While performing numerical simulations of the models given in Section 3.1, the solution did not converge for small values of the liquid conductivity. The value for liquid conductivity, σ_l , reported in White *et al.* [2] is around 2.0 S/m and in Fehribach *et al.* [6] it is around 140 S/m. The model presented here will only admit solutions when the conductivity is well above the value from White *et al.*

The question that arises is whether this is a numerical issue or an ill-posedness of the model.

Using Equation (5),

$$\frac{d}{dx} \left(\sigma_l \epsilon_l(x)^b \frac{d\phi_l}{dx} \right) = \nu_l i_0 c_{\text{O}_2} c_{\text{CO}_2} \exp \left(\frac{n\alpha F(\phi_s - \phi_l)}{RT} \right), \quad (19)$$

we can solve this analytically by non-dimensionalizing the equation according to

$$\bar{\phi}_{l,\bar{x}\bar{x}} - \delta e^{-\bar{\phi}_l} = 0, \quad (20)$$

where

$$\bar{\phi}_l = \frac{n\alpha F}{RT} \phi_l, \quad \bar{x} = L^{-1}x, \quad \delta = \frac{\nu_{\text{CO}_3} L^2}{\sigma_l \epsilon_l(x)^b} \frac{RT}{n\alpha F} i_0 c_{\text{O}_2} c_{\text{CO}_2} e^{\bar{\phi}_s}. \quad (21)$$

In this non-dimensionalized model, the porosity $\epsilon_l(x)$ and solid potential ϕ_s are considered to be constant across the domain, which is a valid assumption based on the results of Chapter 3. The concentration of O_2 and CO_2 are also considered constant across the domain which is a reasonable first-order approximation.

The parameter δ contains the liquid conductivity σ_l . We will now show that a critical value, δ_c , can be found beyond which the steady-state solution will not exist.

4.1 Thermal Runaway

The potential equation, Eq. (20), is similar (replace $\bar{\phi}_l \rightarrow -\bar{\phi}_l$) to the steady-state equation for thermal runaway found in Fowler [7]

$$\theta_{xx} + \lambda e^\theta = 0, \quad (22)$$

with boundary conditions

$$\theta(\pm 1) = 0. \quad (23)$$

This system can be solved analytically as follows: multiply both sides by θ_x and integrate, yielding

$$\int \theta_x \theta_{xx} dx = \int -\lambda e^\theta \theta_x dx, \quad (24a)$$

$$\Rightarrow \frac{1}{2} \theta_x^2 = -\lambda e^\theta + C. \quad (24b)$$

The constant C can be found by imposing the symmetry condition $\theta(-x) = \theta(x)$ and if θ is smooth enough, $\theta_x(0) = 0$. We find $C = \lambda e^{\theta_0}$ where $\theta_0 = \theta(0)$.

Considering only the problem on the interval $x = [0, 1]$ in comparison with Eq. (20), the ODE is re-arranged and the method of separation of variables is applied which gives

$$\theta_x = \sqrt{2\lambda} \sqrt{e^{\theta_0} - e^\theta}, \quad (25a)$$

$$\Rightarrow \int_{\theta_0}^{\theta} \frac{d\theta}{\sqrt{e^{\theta_0} - e^\theta}} = \int_0^x \sqrt{2\lambda} dx = \sqrt{2\lambda} x. \quad (25b)$$

Let us set $z = \sqrt{e^{\theta_0} - e^\theta}$ so that

$$d\theta = -2ze^{-\theta} dz, \quad (26a)$$

$$\Rightarrow \frac{d\theta}{\sqrt{e^{\theta_0} - e^\theta}} = \frac{-2dz}{e^{\theta_0} - z^2}. \quad (26b)$$

Substitution into (25b) gives

$$\sqrt{2\lambda} x = \int_{\theta_0}^{\theta} \frac{d\theta}{\sqrt{e^{\theta_0} - e^\theta}} = -2 \int \frac{dz}{e^{\theta_0} - z^2} = -2e^{-\theta_0/2} \tanh^{-1} \frac{z}{e^{\theta_0/2}}, \quad (27)$$

where we have used the integral [8]

$$\int \frac{du}{a^2 - u^2} = \frac{1}{a} \tanh^{-1} \frac{u}{a}. \quad (28)$$

Re-arranging for z leads to

$$z = \sqrt{e^{\theta_0} - e^\theta} = e^{\theta_0/2} \tanh \left(-\sqrt{\frac{\lambda}{2}} e^{\theta_0/2} x \right) = -e^{\theta_0/2} \tanh \left(\sqrt{\frac{\lambda}{2}} e^{\theta_0/2} x \right), \quad (29)$$

using the identity $\tanh(-x) = -\tanh(x)$. Defining $\gamma = \sqrt{\frac{\lambda}{2}} e^{\theta_0/2} x$, we obtain

$$e^\theta = e^{\theta_0} (1 - \tanh^2 \gamma) = e^{\theta_0} \operatorname{sech}^2 \gamma \quad (30a)$$

or

$$\theta = \theta_0 - 2 \ln \cosh \gamma, \quad (30b)$$

using the identity $1 - \tanh^2 \gamma = \operatorname{sech}^2 \gamma = \cosh^{-2} \gamma$. This solution for θ was found in Fowler [7] and we can use the same approach to solve for the liquid potential.

For this model based on thermal runaway, the maximum temperature, θ_0 , occurs at $x = 0$ (by symmetry), and is determined by satisfying the boundary condition at $x = 1$, $\theta(1) = 0$, and so from (30b)

$$e^{\theta_0/2} = \cosh \left(\sqrt{\frac{\lambda}{2}} e^{\theta_0/2} \right). \quad (31)$$

The solutions to this transcendental equation are studied in Figure 12, which was re-created based on the figure presented in Fowler [7]. Based upon these results, there will either be 2, 1 or 0 solutions depending on whether $\lambda < \lambda_c$, $\lambda = \lambda_c$ or $\lambda > \lambda_c$, respectively. The critical value, λ_c , is found in the following manner.

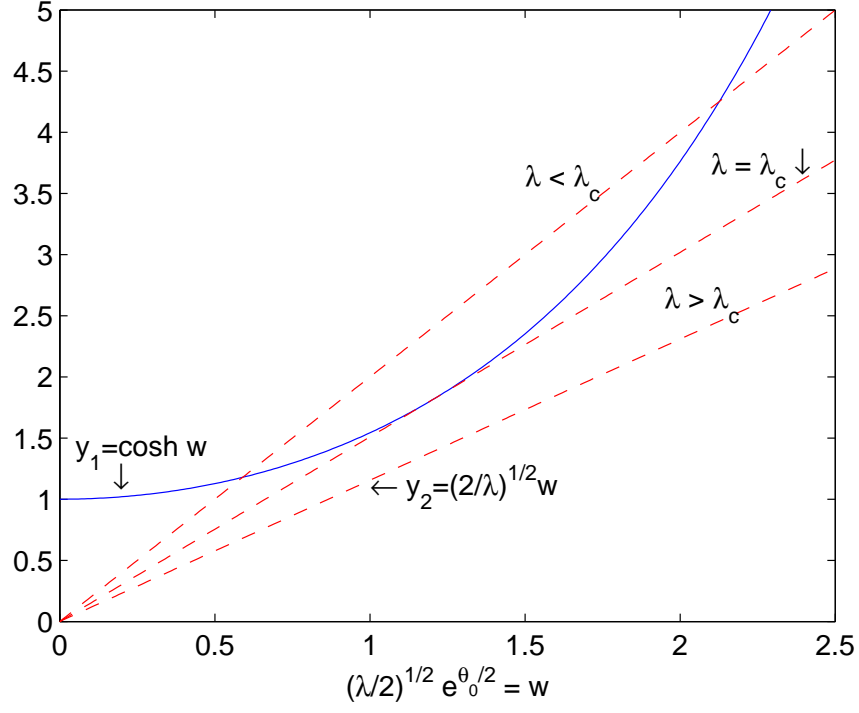


Figure 12: In order to obtain solutions to Eq. (31), the possible solutions based on different values of λ are shown graphically. As λ decreases, the number of solutions increase [7].

Define

$$w = \left(\frac{\lambda}{2}\right)^{1/2} e^{\theta_0/2}, \quad (32)$$

as well as the functions

$$y_1 = \cosh w, \quad (33a)$$

$$y_2 = e^{\theta_0/2} = \left(\frac{2}{\lambda}\right)^{1/2} w. \quad (33b)$$

There exists only one solution if y_2 is tangent to y_1 at some point $w = w^*$. The tangent is given by

$$\frac{d}{dw} \left(\frac{2}{\lambda}\right)^{1/2} w = \frac{d}{dw} \cosh w, \quad (34a)$$

$$\left(\frac{2}{\lambda}\right)^{1/2} = \sinh w, \quad (34b)$$

and point w^* is found from

$$w^* = \left(\frac{\lambda}{2}\right)^{1/2} \cosh w^* = \left(\frac{\lambda}{2}\right)^{1/2} \left(1 + \frac{2}{\lambda}\right)^{1/2} = \left(\frac{\lambda+2}{2}\right)^{1/2}. \quad (35)$$

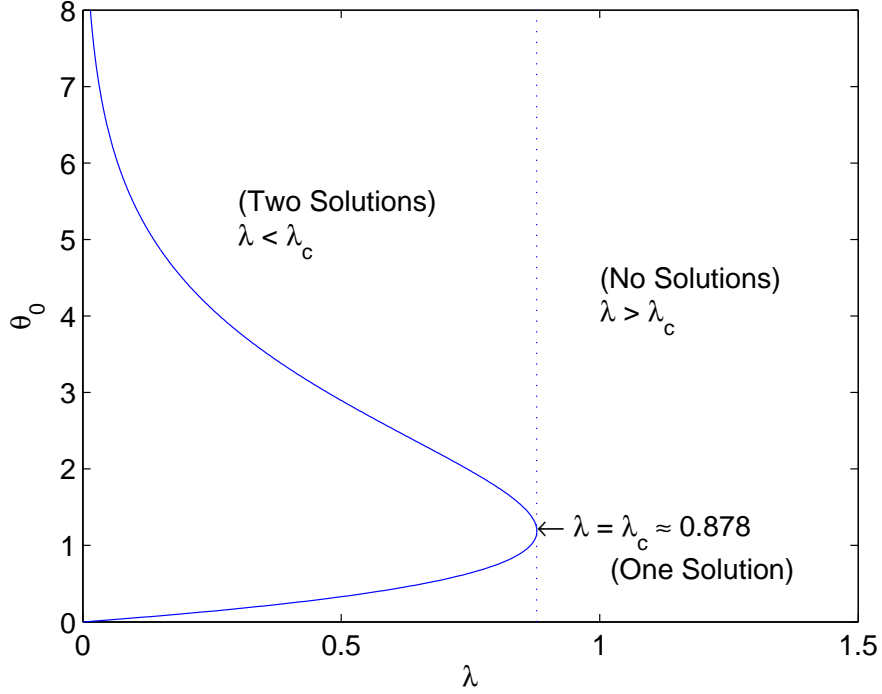


Figure 13: Response diagram for θ_0 as a function of λ . As the value of λ decreases, the value of θ_0 has multiple possibilities that will lead to a steady state solution based on the outcomes of Figure 12 [7].

Upon substitution of (35) into (34b), the critical value, $\lambda_c \approx 0.878$, is given by the unique value that satisfies

$$1 = \sqrt{\frac{\lambda_c}{2}} \sinh \left(\sqrt{\frac{\lambda_c + 2}{2}} \right), \quad (36)$$

which was found using Maple.

Figure 13 gives the value of θ_0 as a function of λ . There exists an asymptote at λ_c , where there are 2 solutions for $\lambda < \lambda_c$, 1 solution for $\lambda = \lambda_c$ or 0 solutions for $\lambda > \lambda_c$.

4.2 Fickian Diffusion

In order to find a solution to expression (20), let $\theta = -\phi_l$ in Eq. (22). Then this system can be solved analytically using the same approach as the one above.

This time, applying the boundary condition at the right boundary ($\phi(1) = 0$) gives the minimum value ϕ_0 which satisfies

$$e^{-\phi_0/2} = \cosh \left(\sqrt{\frac{\delta}{2}} e^{-\phi_0/2} \right). \quad (37)$$

Once again, we can find the critical value, $\delta_c \approx 0.878$, by examining the solutions to Eq. (37) in the same way as Eq. (31). Here, δ_c is given by

$$1 = \sqrt{\frac{\delta_c}{2}} \sinh \left(\sqrt{\frac{\delta_c + 2}{2}} \right). \quad (38)$$

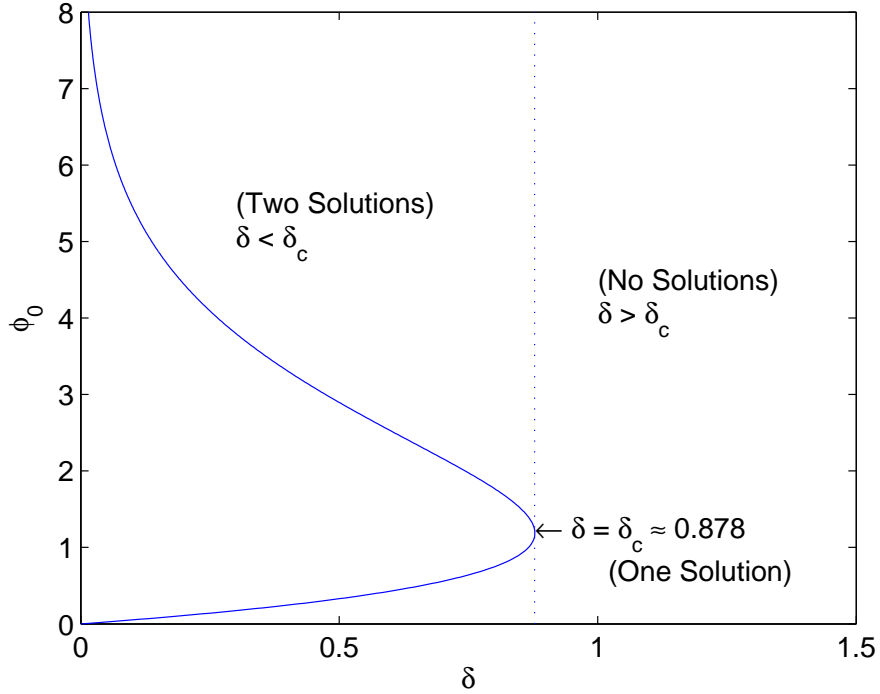


Figure 14: Response diagram for ϕ_0 as a function of δ . The result is the same as for thermal runaway where steady state solutions appear when $\delta \leq \delta_c$.

The solutions are the same and given in Figure 12 where $\theta = -\phi$ and $\lambda = \delta$.

Figure 14 shows the value of ϕ_0 as a function of δ . There exists an asymptote at δ_c , where there are two solutions for $\delta < \delta_c$, one solution for $\delta = \delta_c$ or no solutions for $\delta > \delta_c$. In the case of two solutions, the “high-voltage” solution (i.e., larger value of ϕ_0 for given δ) is very likely unstable (without proof). Therefore, this solution cannot be observed experimentally.

In the MCFC cathode model, as the liquid conductivity decreases, δ will increase (see Eq. (21)). The analytical results presented here explain the non-existence of steady state solutions found in the numerical computations. For large values of D and σ_s , resulting in near constant functions c_{O_2} , c_{CO_2} and ϕ_s , we find very good agreement between the theoretical value of δ_c and the value obtained numerically.

Also, as $\delta \rightarrow \delta_c$, the CPU time increases dramatically.

5 Optimization of a MCFC Cathode

5.1 Full Model Optimization

Initially, the optimization of the porosity in the cathode was attempted for the full model of four variables by using the Fickian Diffusion model with the built-in optimization routines in MATLAB (i.e., `fmincon`). The gas porosity was taken to be a function of the position across the cathode, which affects the results through the Bruggeman term ($\epsilon_i(x)^b$), while the liquid porosity was updated at each position based upon a constant solid porosity. The porosity was updated after convergence to a solution based upon maximizing the current density at the channel. The flux at the channel for the solid potential was used for the maximization criteria.

Results show that either the model is ill-posed or there exists a point where the optimization routine can no longer alter the porosity to reach a maximum for the current. Each time the program was run for the same parameters but different, random initial porosities, the results were inconsistent with each other and were not representative of what was expected based on the physics of the problem. At the channel, it is expected to have a larger porosity than at the electrode/electrolyte interface for the gas porosity to allow for more of the gas species to flow into the electrode and react accordingly. Hence, this optimization approach using `fmincon` was not pursued any further and a different optimization problem was investigated instead, employing optimal control methods.

5.2 Optimal Control

Optimal control problems can be used to measure how effective a given control of a system is by minimizing a cost functional. This type of problem is an important part of optimization and has many applications. The following is a formulation of optimal control problems from Pedregal [9].

The state of a given system is described by a number of parameters,

$$x = (x_1, x_2, \dots, x_n), \quad (39)$$

which evolve according to a state equation,

$$x'(t) = f(t, x(t), u(t)), \quad (40)$$

with boundary or initial conditions

$$x(0) = x_0, \quad x(T) = x_T. \quad (41)$$

The control parameters are given by

$$u = (u_1, u_2, \dots, u_n), \quad (42)$$

and they may depend on t also.

The functional we are attempting to minimize is defined as

$$I(x, u) = \int_0^T F(t, x(t), u(t)) dt. \quad (43)$$

Both the state equation and the objective functional depend upon the control parameters u .

A pair (x, u) is said to be feasible and admissible if the following is fulfilled [9]:

1. constraints on the control: $u(t) \in K$ for all $t \in (0, T)$, where K is the permitted range;
2. state law: $x'(t) = f(t, x(t), u(t))$ for all $t \in (0, T)$;
3. end-point conditions: $x(0) = x_0, x(T) = x_T$.

An optimal control problem may consist of having both or only single endpoint conditions, and transversality conditions may be needed to complete the formulation of the problem, which will be discussed later.

An admissible pair (X, U) is sought such that,

$$I(X, U) \leq I(x, u) \quad (44)$$

for all other feasible pairs (x, u) .

We can incorporate the point-wise constraint Eq. (40) using a Lagrange multiplier or co-state $p(t)$ and consider the augmented functional

$$\bar{I}(x, u, p, x') = \int_0^T [F(t, x(t), u(t)) + p(t) \cdot (f(t, x(t), u(t)) - x'(t))] dt. \quad (45)$$

The optimal solutions for the optimal control problem can be found from the Euler-Lagrange equations for \bar{I} .

Theorem 5.1 (Euler-Lagrange Equation) *If x is an optimal solution of $\int_{\Omega} F(t, x(t), u(t)) dt$, then x must also be a solution of the problem (E-L)*

$$\text{div}(F_x(t, x(t), \nabla x(t))) = F_{\nabla x}(t, x(t), \nabla x(t)) \in \Omega, \quad x = x_0 \in \partial\Omega, \quad (46)$$

for the variables $(x, \nabla x)$ with either prescribed or transversality conditions applied on $\partial\Omega$.

The Euler-Lagrange equations for the optimal control problem can be found first by defining

$$G(t, u, p, x, u', p', x') = F(t, x, u) + p \cdot (f(t, x, u) - x'), \quad (47)$$

where we note that the right-hand side of (47) has no explicit dependence on either u' or p' .

Then the system can be written as

$$\frac{d}{dt} \frac{\partial G}{\partial x'} = \frac{\partial G}{\partial x}, \quad \frac{d}{dt} \frac{\partial G}{\partial u'} = \frac{\partial G}{\partial u}, \quad \frac{d}{dt} \frac{\partial G}{\partial p'} = \frac{\partial G}{\partial p}, \quad (48)$$

and, therefore,

$$-p' = \frac{\partial F}{\partial x}(t, x, u) + p \frac{\partial f}{\partial x}(t, x, u), \quad (49a)$$

$$0 = \frac{\partial F}{\partial u}(x, u, t) + p \frac{\partial f}{\partial u}(t, x, u), \quad (49b)$$

$$0 = x' - f(x, u, t). \quad (49c)$$

Defining the Hamiltonian of the system as $H = F + pf$, we can write

$$p' = -\frac{\partial H}{\partial x}, \quad (50a)$$

$$H(u) = \min_{v \in K} H(v), \quad (50b)$$

$$x' = f(t, x, u). \quad (50c)$$

where K is the set of all admissible controls.

This provides a system of first-order differential equations, (50a) and (50c), for which we need boundary conditions, while (50b) is an algebraic constraint, which includes the end points in the case of a finite domain. We have at least one boundary condition for the equation involving x' , while the boundary condition for p' is completed with the transversality condition or natural boundary condition.

Theorem 5.2 (Transversality Condition) *If at a given endpoint (initial or final) we have a condition on the state, we do not enforce the corresponding transversality condition, but if the state is free, then the transversality condition $p = 0$ at the given endpoint must be taken into account [9].*

This section provides a framework for an optimal control problem involving the diffusion of chemical species across an electrode domain.

5.3 Single Species Optimization

In order to build an optimization routine without the use of built-in functions, a simpler model was introduced that contained only one differential equation that represents a single species diffusing across the domain. Instead of minimizing the current, the objective function consisted of maximizing the reaction rate balanced with a function representing the costs and durability of the electrode. This type of optimization would ensure longevity for the cathode material as well as maximizing the current produced.

Fick's Laws were again used to produce the reaction-diffusion model¹

$$-D \frac{d^2 c}{dx^2} = h(c) = -ac, \quad (51)$$

where D is the control parameter exercised on the system. This parameter will vary across the domain but remains constant to first order and we can avoid taking the derivative with respect to the position in order to complete the optimization. The function $h(c)$ represents the reaction rate and a contains other variables of the system. Since we are using only one equation, we can represent the reactivity, a , as a single constant.

The function $g(D)$, shown in Figure 15 for different values of α , represents the costs and durability of the cathode material

$$g(D) = \alpha (D - D_0)^2. \quad (52)$$

The objective function will measure how good the control is based upon the criteria discussed above. It is given by

$$I(c, D) = \int_0^L \lambda h(c) + (1 - \lambda)g(D) dx. \quad (53)$$

Here, λ can be between 0 and 1, but chosen to be 0.5. If λ is 1, it turns out that the objective function cannot be minimized as the optimization fails. If λ is 0, the objective function is no longer maximizing the reaction rate.

The parameter α is increased to prevent the diffusion coefficient from becoming too large or too small in the optimization process. If we have a large diffusion coefficient, the porous medium no longer has an effect on the diffusion across the domain. It also means that the electrode is more porous and less stable mechanically. Note that D cannot exceed the diffusivity in bulk gas. A small diffusion coefficient would require smaller pores which are difficult to manufacture for the same volume fraction of species, resulting in high costs. Therefore, as the optimization routine processes, the diffusion coefficient remains in the vicinity of the minimum value, D_0 . Here, we choose $D_0 = 1$.

The boundary conditions are both considered at the origin, which represents the electrode/electrolyte interface where the gas cannot flow across

$$c(0) = c_0, \quad \frac{dc}{dx}(0) = 0. \quad (54)$$

As the species diffuses from right to left in the domain (Figure 16), we expect the concentration to reach a specified value, c_0 , while maintaining no flux at the left boundary into the electrolyte.

¹Strictly speaking, we need to solve $-\frac{d}{dx} \left(D(x) \frac{dc}{dx} \right) = -\frac{dD}{dx} \frac{dc}{dx} - D \frac{d^2 c}{dx^2} = -ac$. Hence, we shall see that for large α in (52), the term $-\frac{dD}{dx} \frac{dc}{dx}$ can be neglected. As α decreases, the term gains in importance. Future work will include the optimization of the full model $-\frac{d}{dx} \left(D(x) \frac{dc}{dx} \right) = -ac$, possibly by utilizing the routine `fmincon` in MATLAB or other commercial software.

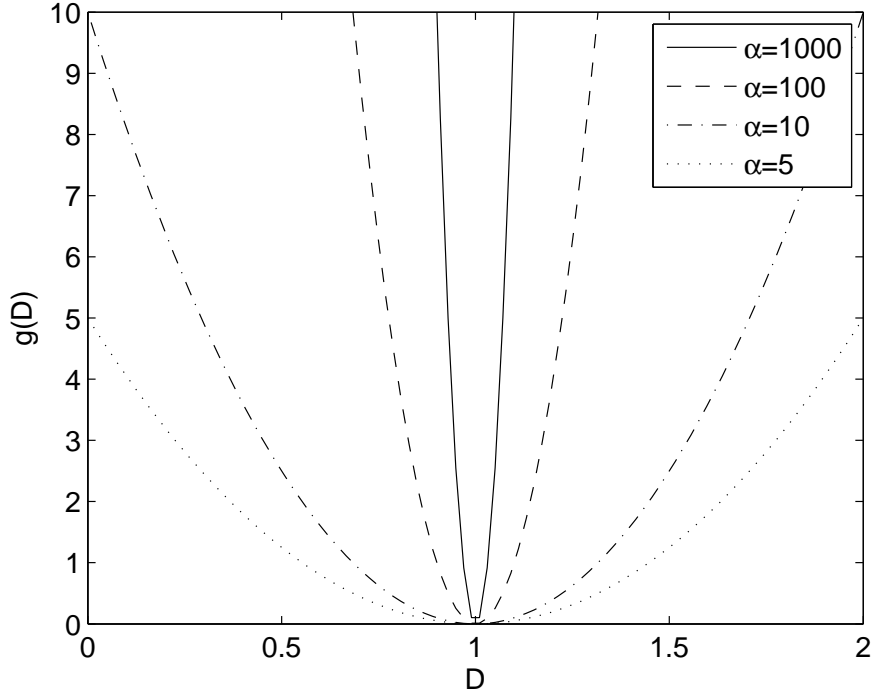


Figure 15: Function to be minimized representing the costs and durability of the cathode materials. If the diffusivity, D , is increased, the porous medium becomes less durable. If the diffusivity is decreased, the pore size becomes much smaller and is harder to manufacture for the same volume fraction of species. In order to stay near the optimal value (minimum D), the parameter α is increased.

The channel is considered to be at the right boundary. The Dirichlet condition ($c(0) = c_0$), which is typically found at the channel ($x = L$) is moved to the electrolyte interface so as to have a well-defined optimization problem.

Using the method described in Section 5.2, we start by formulating the second-order differential equation, Eq. (51), as two first-order differential equations with corresponding boundary conditions,

$$x'_1 = x_2, \quad x_1(0) = c_0, \quad (55)$$

$$x'_2 = -\frac{h(x_1)}{D}, \quad x_2(0) = 0, \quad (56)$$

where the Hamiltonian is given by,

$$H = \lambda h(x_1) + (1 - \lambda)g(D) + px_2 - \frac{qh(x_1)}{D}. \quad (57)$$

Here, p and q are co-states of x'_1 and x'_2 .

Using the Hamiltonian, a system of equations is defined based upon the Euler-Lagrange system,

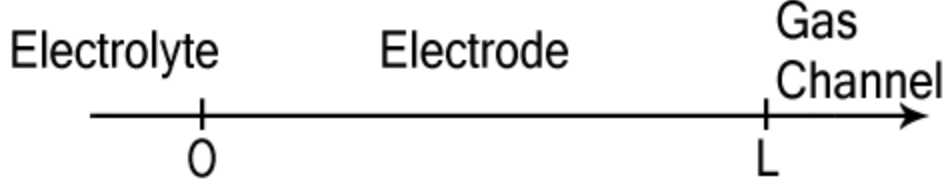


Figure 16: Domain schematic for the simplified model (51)-(54).

Eqs. (50a)-(50c),

$$p' = -\frac{\partial H}{\partial x_1} = -\left(\lambda h'(x_1) - \frac{qh'(x_1)}{D}\right) = -h'(x_1)\left(\lambda - \frac{q}{D}\right), \quad (58a)$$

$$q' = -\frac{\partial H}{\partial x_2} = -p, \quad (58b)$$

$$H(D) = \min_{v \in K} H(v) = \min_{v \in K} \left[\lambda h(x_1) + (1 - \lambda)g(v) + px_2 - \frac{qh(x_1)}{v} \right], \quad (58c)$$

$$\Rightarrow D^2(D - D_0) = \frac{-qh(x_1)}{\alpha}, \quad (58d)$$

where we used $\lambda = 1/2$.

The transversality conditions for this problem are given at the channel,

$$p(L) = q(L) = 0. \quad (59)$$

The solution will generally require numerical tools. However, the problem will first be simplified in order to achieve an analytical solution of the system of four ODEs, including the algebraic equation (58d).

In our simple model, let $a = c_0 = L = D_0 = 1$ and $\lambda = \frac{1}{2}$. Then Eqs. (55), (56), (58a) and (58b) become

$$x_1' = x_2, \quad (60a)$$

$$x_2' = \frac{x_1}{D}, \quad (60b)$$

$$p' = \frac{1}{2} - \frac{q}{D}, \quad (60c)$$

$$q' = -p, \quad (60d)$$

with boundary conditions

$$x_1(0) = 1, \quad x_2(0) = 0, \quad p(1) = 0, \quad q(1) = 0. \quad (61)$$

In Eqs. (60b) and (60c), D is determined by Eq. (58d), which couples all four equations (60a)-(60d). We see that as $\alpha \rightarrow \infty$, $D \rightarrow 1$ across the domain since $D = 0$ is not permissible. Setting $D \equiv 1$ decouples the four equations into 2 pairs of equations. This is acceptable as a first-order approximation to find an analytical solution since we will see that this is consistent for small α as well. Therefore, we first solve

$$x_1' = x_2, \quad x_1(0) = 1, \quad (62a)$$

$$x_2' = x_1, \quad x_2(0) = 0, \quad (62b)$$

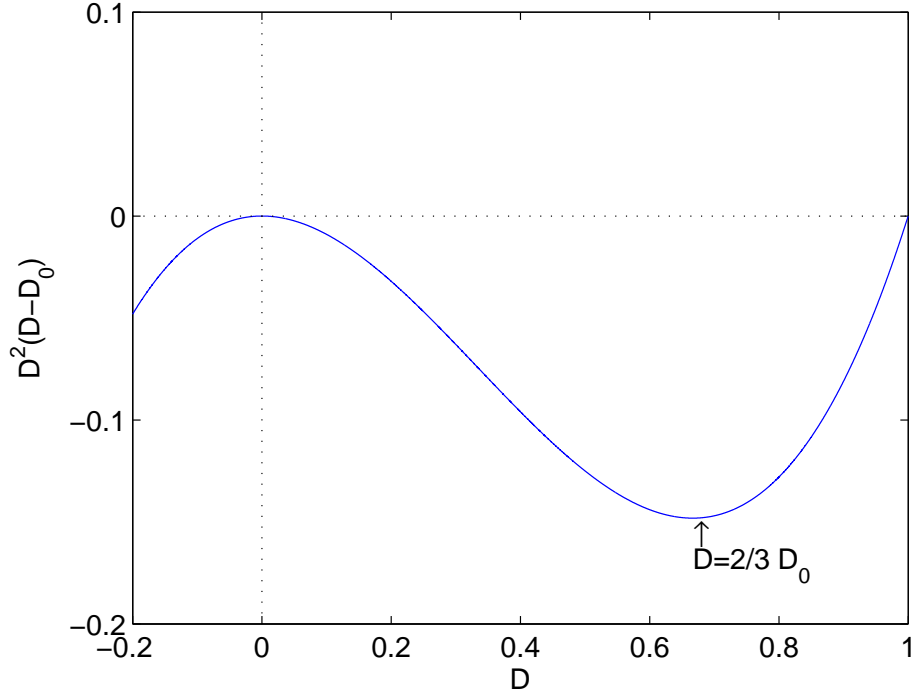


Figure 17: The diffusion coefficient will always be a positive-valued number, which is determined by Eq. (58d). The smallest value of D will occur at the electrode/electrolyte boundary where the gas can no longer diffuse. The minimum value, \hat{D} , is found where there exists a local minimum in Eq. (58d) as shown on the graph.

which yields the general solutions

$$x_1(x) = C_1 \sinh(x) + C_2 \cosh(x), \quad (63a)$$

$$x_2(x) = C_1 \cosh(x) + C_2 \sinh(x). \quad (63b)$$

Applying the boundary conditions gives the final solutions

$$x_1(x) = \cosh(x), \quad (64a)$$

$$x_2(x) = \sinh(x). \quad (64b)$$

Similarly, we solve the remaining two ODEs

$$p' = \frac{1}{2} - q, \quad p(1) = 0, \quad (65a)$$

$$q' = -p, \quad q(1) = 0. \quad (65b)$$

This gives the following solutions

$$p(x) = C_1 \sinh(x) + C_2 \cosh(x), \quad (66a)$$

$$q(x) = \frac{1}{2} - (C_1 \cosh(x) + C_2 \sinh(x)). \quad (66b)$$

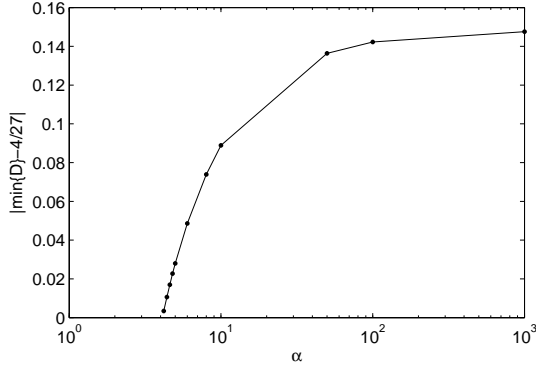


Figure 18: As the value of α decreases in $g(D)$, the solution begins to diverge as the local minimum of D is passed.

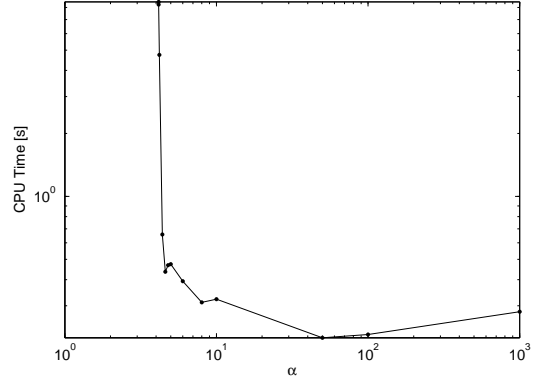


Figure 19: As the value of α_c is approached, the CPU time begins to increase exponentially as it becomes much more difficult to reach a steady state solution numerically.

Applying the boundary conditions leads to the two conditions

$$p(1) = 0 = C_1 \sinh(1) + C_2 \cosh(1), \quad (67a)$$

$$q(1) = 0 = \frac{1}{2} - C_1 \cosh(1) - C_2 \sinh(1) \quad (67b)$$

with solutions $2C_1 = \cosh(1)$ and $2C_2 = -\sinh(1)$. Applying these constants to p and q , one finds that

$$p(x) = \frac{1}{2} \cosh(1) \sinh(x) - \frac{1}{2} \sinh(1) \cosh(x), \quad (68a)$$

$$q(x) = \frac{1}{2} - \frac{1}{2} \cosh(1) \cosh(x) + \frac{1}{2} \sinh(1) \sinh(x). \quad (68b)$$

The solutions to the system of ODEs in the limit $\alpha \rightarrow \infty$ are given in equations (64a)-(64b) and (68a)-(68b).

In order to solve this problem numerically for general α , a shooting method is used. Based upon the analytical results found here for $\alpha \rightarrow \infty$, an initial guess can be obtained from $p(0)$ and $q(0)$

$$p(0) = -\frac{1}{2} \sinh(1) < 0, \quad q(0) = \frac{1}{2} (1 - \cosh(1)) < 0. \quad (69a)$$

Hence, we start in the 3rd quadrant of the (p, q) - plane and need to end up at the origin when $x = 1$.

A secant method is used to update the guess for the next iteration for α which needs two initial guesses. The second guess is chosen to be within 1% of the first initial guess so as not to stray away from the analytical results. By choosing the solution of the previous α as the next initial guess, α can be varied and decreased step-by-step, and the solutions can be found. Note that we are strictly shooting in four dimensions, equivalent to a four-dimensional surface embedded in five dimensions owing to the algebraic constraint (58d). The algebraic equation is solved using a built-in MATLAB root solver, `fzero`, after every iteration.

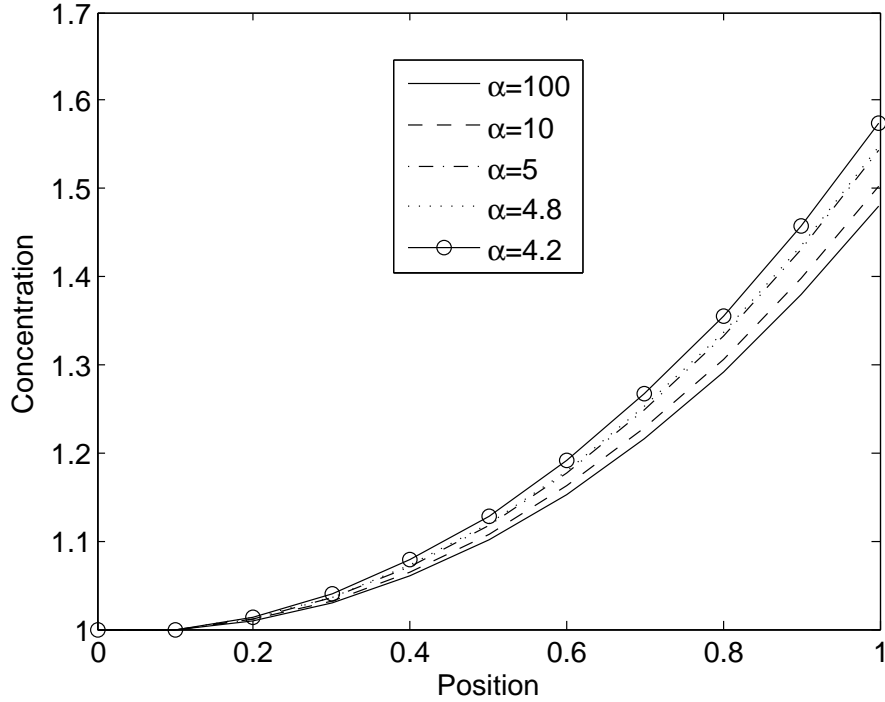


Figure 20: The concentration profile across the domain for decreasing values of α . As the value of α_c is approached, the solution remains within the same order of magnitude.

In order for the solution to converge, the right-hand side of Eq. (58d) cannot drop below the local minimum of the left-hand side or else D would be negative which is unphysical. The minimum, \hat{D} , is found from,

$$\frac{d}{dD} \left(\hat{D}^2 (\hat{D} - D_0) \right) = 0, \quad (70a)$$

$$\Rightarrow 3\hat{D}^2 - 2\hat{D}D_0 = 0, \quad (70b)$$

$$\Rightarrow \hat{D} = \frac{2}{3}D_0, \quad (70c)$$

where $D_0 = 1$ is chosen so as to simplify the system. The value, D_0 , will occur at the right boundary since we have $q(1) = 0$ in (58d). The diffusivity as a function of x is found using a root finder at each point, using (58d) and the solutions for q and x_1 . The minimum of $\frac{2}{3}D_0$ will occur close to some critical value of α , which is the lowest possible value where the numerical solution does not exist, and represents the smallest possible value of D and α , as seen in Figure 17. The minimum value of D decreases monotonically with α . The difference between the numerical minimum value, $\min\{D\}$, and the analytical value, $\left(\frac{2}{3}\right)^2 \left(\frac{2}{3} - 1\right) = -\frac{4}{27}$, is shown in Figure 18.

Numerically to four decimal places, the critical value of α was computed as 4.1558. As the critical value is approached from above, the CPU time increases without bound as in Figure 19. As $\alpha \rightarrow \alpha_c$, the solution approaches the graph shown in Figure 20.

Finally, we would like to gauge whether dropping the term $-\frac{dD}{dx} \frac{dc}{dx}$ in deriving (51) is justified. The presence of this term would modify Eq. (51) to give

$$-\frac{dD}{dx} \frac{dc}{dx} - D \frac{d^2c}{dx^2} = -ac. \quad (71)$$

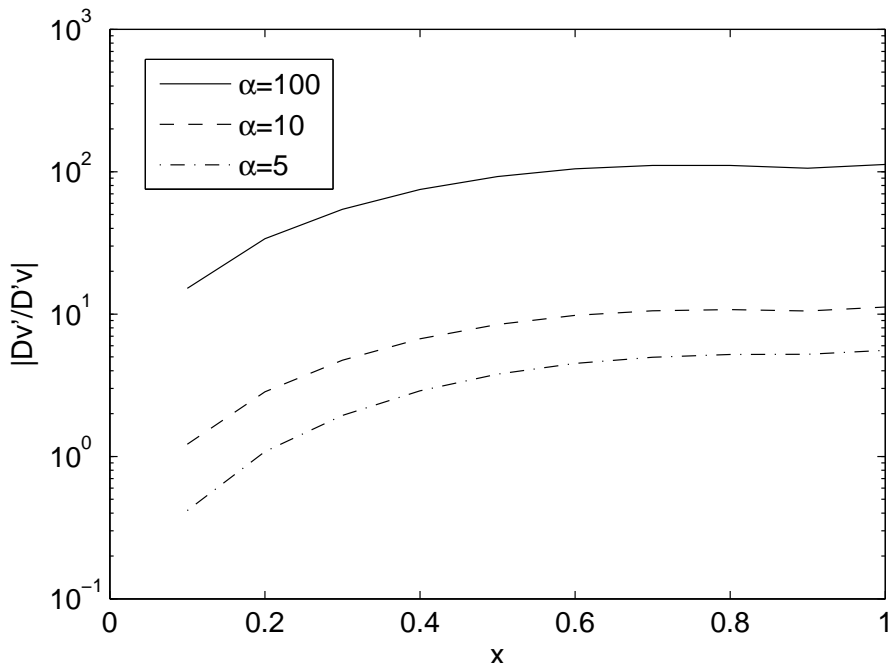


Figure 21: Comparison of the two terms on the left-hand side of (71). For large α , the ratio is large and the model (51) seems justified. As α decreases, the extra term in the full model (71) becomes increasingly important.

For $a = 1$, the two terms on the left-hand side can be compared by their ratio $\left| \frac{Dc''}{D'c'} \right|$. However, the presence of this additional term renders our optimization method non-applicable.

Regardless of this fact, we are plotting in Figure 21 this ratio for different values of α , approximated by our solution of the optimization problem $x_1(x)$, $x_2(x)$, $D(x)$ and so

$$\left| \frac{Dc''}{D'c'} \right| = \left| \frac{Dx'_2}{D'x_2} \right|. \quad (72)$$

We see that for large α , our original simplification in deriving (51) seems justified. However, as $\alpha \rightarrow \alpha_c$ we can observe that the term $\frac{dD}{dx} \frac{dc}{dx}$ plays an increasingly important role and, in principle, the full model needs to be optimized, i.e., Eq. (71).

6 Conclusion and Future Work

Three different models of diffusion across the cathode of a MCFC based on Fickian diffusion, convection-diffusion and multicomponent diffusion with convection were studied. It has been shown that the results can differ significantly, depending on system parameters.

The convection-diffusion model shows that for standard values found from the literature, the convective flux dominates the gas species' total flux across the domain. This is a significant result since this phenomenon has not been taken into account by other researchers such as White *et al.* [2] and should be included in any model of mass transport for a MCFC. Since the convective flux is the dominant term, an approximation using only Fickian diffusion with an effective diffusivity is not possible as diffusion will only model a decrease in concentration towards the electrolyte.

The Maxwell-Stefan equations for multicomponent diffusion take into consideration the momentum losses due to the interactions between particles of different species. Combining it with the convective flux gives a more detailed view of the mass transport inside the cathode. For the standard values from the literature, the results of the multicomponent model follow those of the simpler convection-diffusion model with very high accuracy. In other words, the convection-diffusion model is a good approximation of the more complex binary diffusion model. At low values of the permeability, the convective flux approaches zero, which allows the differences between the models to become apparent since the diffusive fluxes do (simple diffusion) or do not (multi-component diffusion) add up to zero.

While performing the numerical simulations for values of the liquid conductivity obtained from the literature, a steady-state solution could not be achieved for small values. By using a simpler problem, an analytical solution was derived showing that there exists a critical value for the liquid conductivity below which steady-state solutions do not exist. This is another significant result as it shows that not only convection needs to be included in the White *et al.* [2] model but the parameter values are inconsistent.

The optimization of the electrode for a fuel cell is of great importance as it will aid in the manufacturing of cell components to improve cell performance as well as increase life time. An analytical solution has been derived for a simplified system that involves the optimal profile of the diffusivity across the domain as a control on the cathode. The diffusivity can be varied in the more comprehensive models using the porosity profile across the domain. Using the data obtained from the optimization routine, both analytical and numerical, the porosity may be manufactured so as to improve the performance and life time of the cell.

Future work depends upon the availability of parameters that will help to better understand the convection-diffusion results. As the fuel cell begins to reach market acceptance, the optimization of the fuel cell will grow in importance and will aid in the manufacturing of cell components to further increase the viability of the MCFC. A more realistic optimization of the cathode transport processes needs to be investigated.

Acknowledgement

We would like to thank Enbridge Inc. for their funding and support through the Ontario Fuel Cell Research and Innovation Network.

References

- [1] X. Li, *Principles of Fuel Cells*, (Taylor & Francis Group, 2006)
- [2] N. Subramanian, B. S. Haran, R. E. White and B. N. Popov, B. N., *Full Cell Mathematical Model of a MCFC*, J. Electrochem. Soc. **150**, A1360 (2003)
- [3] D. A. G. Bruggeman, *Berechnung verschiedener physikalischer Konstanten von heterogenen Substanzen. I. Dielektrizitätskonstanten und Leitfähigkeiten der Mischkörper aus isotropen Substanzen*, Ann. Phys. Leipzig **416**, 665 (1935)
- [4] K. Promislow, P. Chang, H. Haas and B. Wetton, *Two-Phase Unit Cell Model for Slow Transients in Polymer Electrolyte Membrane Fuel Cells*, J. Electrochem. Soc. **155**, A494 (2008)
- [5] E. L. Cussler, *Diffusion, Mass Transfer in Fluid Systems*, (Cambridge University Press, 1984)
- [6] J. A. Prins-Jansen, J. D. Fehribach, K. Hemmes and J. H. W. de Wit, *A Three-Phase Homogeneous Model for Porous Electrodes in Molten-Carbonate Fuel Cells*, J. Electrochem. Soc. **143**, 1617 (1996)
- [7] A. C. Fowler, *Mathematical Models in the Applied Sciences*, (Cambridge University Press, 1997)
- [8] G. Grosche, V. Ziegler and D. Ziegler, *Taschenbuch der Mathematik*, (B. G. Teubner Verlagsgesellschaft, 1991)
- [9] P. Pedregal, *Introduction to Optimization*, (Springer-Verlag, 2004)
- [10] U. M. Ascher and L. R. Petzold, *Computer Methods for Ordinary Differential Equations and Differential-Algebraic Equations*, (SIAM, 1998)
- [11] C. F. Curtiss and R. B. Bird, *Multicomponent Diffusion*, Ind. End. Chem. Res. **38**, 2515 (1999)
- [12] National Energy Technology Laboratory and U.S. Department of Energy, *Fuel Cell Handbook*, (University Press of the Pacific, 2005)
- [13] J. D. Sole, *Investigation of Water Transport Parameters and Processes in the Gas Diffusion Layer of PEM Fuel Cells*, (Virginia Polytechnic Institute and State University, 2008)
- [14] R. Taylor and R. Krishna, *Multicomponent Mass Transfer*, (Wiley-Interscience, 1993)
- [15] P. Tomczyk, *MCFC versus other fuel cell - Characteristics, technologies and prospects*, J. Power Sources **160**, 858 (2006)